

Strong anisotropy of hole subbands in (311) GaAs-AlAs quantum wells

E. C. Valadares

Department of Physics, University of Nottingham, Nottingham NG7 2RD, United Kingdom

(Received 26 February 1992)

Strong anisotropy features (e.g., saddle points) displayed by excited states of (311) valence-band GaAs-AlAs quantum wells are determined through the exact solution of the effective-mass equation including the spin-orbit interaction. Qualitative changes in the topology of the subband energy surfaces occur as the well width is varied. The relevance of the present calculations for the interpretation of recent resonant magnetotunneling experiments on *p*-type (311)A double-barrier heterostructures is discussed.

I. INTRODUCTION

The study of optical and transport properties of high-quality *p*-type semiconductor quantum-well (QW) heterostructures grown along lower symmetry directions has recently aroused considerable interest because of their technological possibilities and for providing a source of basic research. Hayakawa *et al.*¹ reported that the threshold of single-quantum-well (SQW) lasers can be lowered by using (111)B surfaces. Mobility enhancements of a two-dimensional hole gas (2DHG) have been observed by Davies *et al.*² in modulated *p*-type GaAs/(AlGa)As heterostructures grown on the (311)A GaAs surface. Such high-quality samples allowed them to study the fractional quantum Hall effect (FQHE) for holes. Evidence of a weak hole Wigner crystal in a GaAs/AlGaAs structure grown on an undoped GaAs (311)A substrate and modulation doped with Si has also been reported.³

Recently, the resonant magnetotunneling spectroscopy (RMTS) technique has been used to map out the dispersion curves of *p*-type (100) QW's.⁴ It has also been used to probe the conduction-band anisotropy of *n*-type QW's,⁵ and more recently, to study anisotropy effects in strained Si/Si_{1-x}Ge_x quantum wells.⁶ By using this technique to probe *p*-type AlAs/GaAs (311)A tunneling devices along different in-plane directions, a saddle-point ("camel's back") structure in the energy versus in-plane momentum dispersion curves $E(k_{||})$ for one of the subbands of the valence quantum well has been mapped out in recent experiments.⁷

In this paper we present an exact solution of the effective-mass equation including the spin-orbit (SO) interaction for an isolated QW under flat band conditions grown in a general crystal plane direction. We investigate the anisotropy of hole subbands in (311) valence-band QW's pointing out the usefulness of flat band calculations to interpret the dispersion curves probed by RMTS. Remarkably, (311) AlAs/GaAs/AlAs wells display a much richer variety of anisotropic energy surfaces compared with (100) QW's, whose subbands are much less anisotropic.⁸

II. FORMALISM

Our treatment is a natural extension of the formalism proposed by Andreani, Pasquarello, and Bassani,⁹ which

does not include the SO interaction. We adopt, however, a procedure based on the transfer-matrix technique which is more suitable for QW's grown along lower symmetry directions, especially when the effective-mass Hamiltonian lacks inversion symmetry. Our starting point is the 6×6 Luttinger Hamiltonian for the bulk in its standard representation,¹⁰ $H_B(k_x, k_y, k_z)$, where k_x , k_y , and k_z are the components of the \mathbf{k} wave vector along the cubic axes of the crystal. The explicit form of H_B is given in Appendix A, relation (A1). The QW problem is solved by considering the solution of the effective-mass equation in each bulk semiconductor.¹¹ Let k_1 , k_2 , and k_3 , be the components of \mathbf{k} such that k_3 is along the sample growth direction. k_x , k_y , and k_z are related to k_1 , k_2 , and k_3 by a simple rotation, namely,

$$\begin{aligned} k_x &= x_1 k_1 + x_2 k_2 + x_3 k_3, \\ k_y &= y_1 k_1 + y_2 k_2 + y_3 k_3, \\ k_z &= z_1 k_1 + z_2 k_2 + z_3 k_3, \end{aligned} \tag{1}$$

where for a (311) substrate k_3 is along the (311) direction and k_1 and k_2 are taken along the $(\bar{2}, 3, 3)$ and $(0, \bar{1}, 1)$ directions, respectively, with $k_j (j=1, 2, 3) = -i\nabla_j (\hbar=1)$.

The Hamiltonian for the QW problem is obtained by substituting (1) into $H_B(k_x, k_y, k_z)$ and adding the confining potential:

$$H = H'_B(k_1, k_2, k_3) + V(Z), \tag{2}$$

where Z is along the (311) direction and $V(Z)$ vanishes inside the well ($-L_w/2 < Z < L_w/2$) and equals $-V_0$ in the barriers.

We adopt essentially the same considerations used by Andreani, Pasquarello, and Bassani,⁹ taking into account that we now have a six-component envelope function $\underline{F} = (F_1, F_2, F_3, F_4, F_5, F_6)$ which satisfies the effective-mass equation $H\underline{F} = E\underline{F}$. The boundary conditions require continuity of the components of \underline{F} and $J_3 \underline{F}$ at each interface, where J_3 is the Z component of the probability flux operator. J_3 is formally obtained by taking the derivative with respect to k_3 of each element of the kinetic matrix operator $H'_B(k_1, k_2, k_3)$ and substituting $k_3 = -i\nabla_3 \equiv -id/dZ$ in the resulting matrix expression. The values of k_3 compatible with a given energy E and in-plane component $k_{||} = (k_1, k_2)$ are the roots of the

sixth-order polynomial equation in k_3 obtained by substituting (1) into the secular equation for $H_B(k_x, k_y, k_z)$, relation (A2). To calculate the energy levels $E(k_{\parallel})$ we use the flat band condition of the heterostructure potential. For each E we find the eigenfunctions of the Luttinger Hamiltonian with a given k_{\parallel} and with the corresponding values of k_3 , as indicated in Appendix A. Finally, we construct four 12×12 matrices related to the wave function and the probability flux in both barriers and inside the QW. By ordering the corresponding matrices for the barriers as prescribed in Appendix B we end up with a 6×6 determinantal equation obtained from the total transfer matrix of the heterostructure T relating the twelve coefficients of the wave-function expansion in the left (L) barrier with those in the right (R) barrier. We have thus to invert two 12×12 matrices and calculate a 6×6 determinant which gives the subband dispersion in an implicit form.

III. DISCUSSION OF THE NUMERICAL RESULTS

We have adopted the following values for the Luttinger parameters and the split-off energy¹² in our calculations: $\gamma_1=6.85$, $\gamma_2=2.1$, $\gamma_3=2.9$, and $\Delta=340$ meV for GaAs and $\gamma_1=3.45$, $\gamma_2=0.68$, $\gamma_3=1.29$, and $\Delta=275$ meV for AlAs. There has been some spread in the reported experimental values of these parameters for GaAs,¹³ especially for γ_2 . A discussion of this point in connection with the QW problem will be presented below. The dependence of $E(k_{\parallel}=0)$ on the well width, for $36 \text{ \AA} \leq L_W \leq 80 \text{ \AA}$ and $V_0=550$ meV (AlAs barrier) is shown in Fig. 1. For the first four bound states, by increasing L_W the distance between neighboring states continuously decreases, as in the electronic case. However, for holes this means a stronger mutual interaction between subbands. It should be noted that even for $k_{\parallel}=0$ there is some mixing between hole states contrary to the case of (100) QW's,⁹ since the kinetic matrix Hamiltonian for a [311] QW has finite nondiagonal elements. For states of higher energy there is an ex-

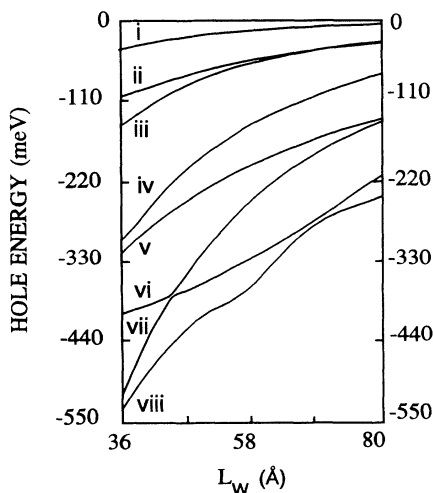


FIG. 1. Hole energy at $k_{\parallel}=0$ vs L_W for an isolated AlAs/GaAs/AlAs (311) QW (Luttinger parameters and split-off energy according to Ref. 12).

tra interaction with the split-off band ($\Delta=340$ meV). There are two conspicuous nontrivial anticrossings for $L_W \simeq 45$ and 68 \AA between the sixth (vi) and seventh (vii) bound states and between the seventh (vii) and eighth (viii) bound states, respectively. The complex interaction between hole states is particularly demonstrated in the case of the fourth (iv) bound state for increasing values of L_W , since it becomes equidistant from its neighbor and next-neighbor bound states, which in their turn approach asymptotically (anticross) each other. Figure 2 shows the dispersion curves $E(k_{\parallel})$ along two orthogonal in-plane directions for a (311) QW with $L_W=42$ and 60 \AA . These QW's illustrate the general trend of $E(k_{\parallel})$ with increasing L_W . It is clear from Fig. 2 that the ground state for both QW's does not exhibit any significant anisotropy.¹⁴ In the case of the 42- \AA well, the fourth (iv) hole subband is the one which presents the most significant anisotropy

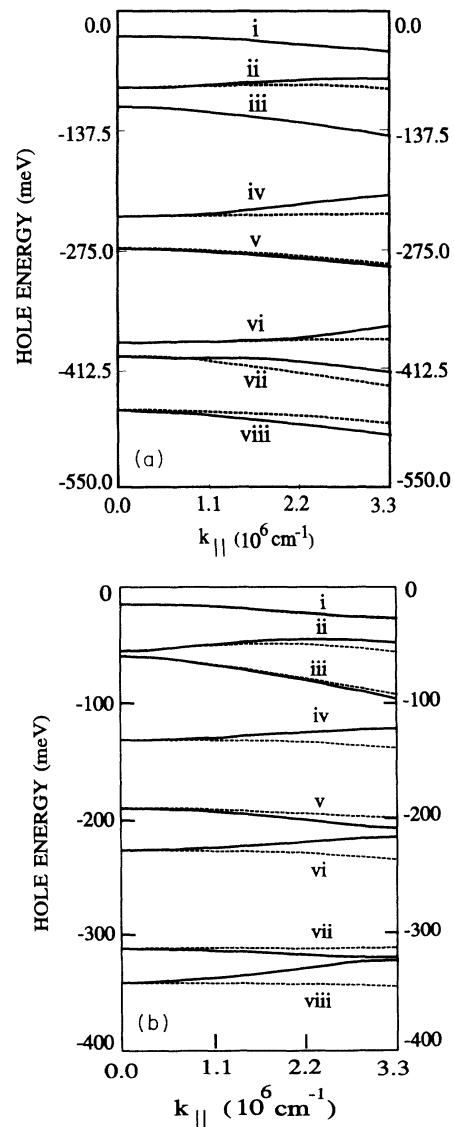


FIG. 2. Hole dispersion curves for an isolated AlAs/GaAs/AlAs QW with $L_W=42 \text{ \AA}$ (a) and $L_W=60 \text{ \AA}$ (b) in zero electric and magnetic fields. The continuous line refers to the $(0\bar{1}1)$ direction and the dashed line to the $(\bar{2}33)$ direction.

among the first five dispersion energy surfaces: along the $(\bar{2}33)$ direction $E_{iv}(k_{\bar{2}33})$ is relatively flat, whereas along the $(0\bar{1}1)$ direction $E_{iv}(k_{0\bar{1}1})$ has a much more pronounced negative curvature (negative effective mass). As L_W is increased $E_{iv}(k_{\bar{2}33})$ becomes even flatter and eventually its curvature becomes positive (positive effective mass), whereas the curvature of $E_{iv}(k_{0\bar{1}1})$ remains negative for greater L_W .

The form of the subband energy surface $E_{iv}(k_{\parallel})$ depends critically on L_W . For $L_W = 60 \text{ \AA}$, $E_{iv}(k_{\parallel})$ exhibits a clear-cut saddle point with the biaxial symmetry of the crystal, as depicted in Fig. 3. The corresponding density of states has three maxima: at the saddle point ($k_{\parallel} = 0$),¹⁵ which may produce a distinct optical signal in photoluminescence experiments, and at the two energies indicated in Fig. 3. These two extra maxima also reflect the anisotropy of this subband, since the E_{iv} energy surface attains two distinct plateaus for higher values of k_{\parallel} along the $(\bar{2}33)$ and $(0\bar{1}1)$ directions, not depicted in the figure. The sixth subband E_{vi} also presents a saddle-point structure, as is evident from Fig. 2(b). By comparing the whole set of dispersion curves for the two QW's we notice two basic differences: change of curvatures and relative separation of the subbands. Both these qualitative features are probed by the RMTS technique.^{4,7}

We have also investigated the existence of saddle points for QW's with $L_W < 60 \text{ \AA}$ by varying γ_2 for GaAs and keeping γ_1 and γ_3 fixed as well as the γ parameters for the barrier. For barriers high enough, as in our case, the QW subbands are less sensitive to changes in the latter. For instance, the energy surfaces $E_{iv}(k_{\parallel})$ and $E_{vi}(k_{\parallel})$ of a 48- \AA -wide well exhibit a saddle point in the range $2.4 < \gamma_2 < 2.6$. The energy surfaces are approximately paraboloids with negative curvature for $\gamma_2 < 2.4$ and paraboloids with positive curvature for $\gamma_2 > 2.6$. The topology of the energy surfaces of E_{iv} and E_{vi} is thus very sensitive on the value of γ_2 . These qualitative features and the overall differences in curvature and relative separation of subbands could be exploited to determine the Luttinger γ parameters by fitting the experimental dispersion curves of a p -type (311) QW.⁷

In the RMTS technique it is important that the magnetic length $l_B > L_W$ in order to avoid significant distortions of the measured dispersion curves, in which case the magnetic field B basically transfers in-plane momentum to the tunneling holes.⁴ Also, in narrow QW's an applied bias produces a rigid shift of the hole subbands.¹⁶ Furthermore, the QW dispersion curves for finite width barriers are the same as discussed here provided the barriers are thick enough.⁴

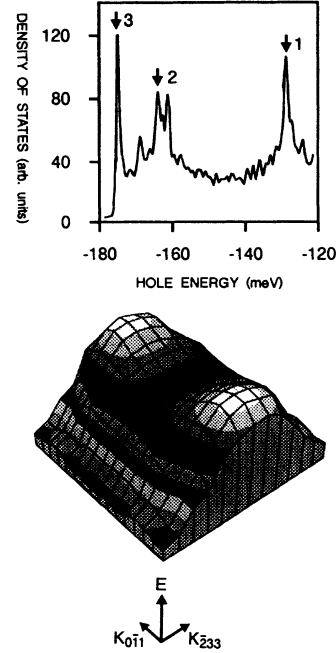


FIG. 3. Saddle point displayed by the fourth (iv) subband of Fig. 2(b) and the corresponding density of states (DOS). Arrow number 1 indicates the saddle-point energy (see text). The lack of smoothness of this curve is due to the method used to calculate the DOS, based on a histogram counting of states.

IV. CONCLUSIONS

In summary, we have determined a saddle-point structure in the hole subband energy surfaces of an isolated (311) QW under flat band conditions by solving exactly the effective-mass equation including the SO interaction. The formalism can be used to treat more complex potentials by digitizing them and using the transfer-matrix technique. Also, the exact wave function can be used as a good starting point to treat excitons confined in QW's and to model coherent¹⁷ and sequential hole tunneling.¹⁶

ACKNOWLEDGMENTS

The author is indebted to F. W. Sheard, L. Eaves, and U. Ekenberg for helpful discussions. Financial support from the Brazilian Research Council (CNPq) is also gratefully acknowledged.

APPENDIX A

The Luttinger Hamiltonian for the bulk including the spin-orbit interaction reads¹⁰

$$H_B = - \begin{pmatrix} P+Q & L & M & 0 & iL/\sqrt{2} & -i\sqrt{2}M \\ L^+ & P-Q & 0 & M & -i\sqrt{2}Q & i\sqrt{\frac{3}{2}}L \\ M^+ & 0 & P-Q & -L & -i\sqrt{\frac{3}{2}}L^+ & -i\sqrt{2}Q \\ 0 & M^+ & -L^+ & P+Q & -i\sqrt{2}M^+ & -iL^+/\sqrt{2} \\ -iL^+/\sqrt{2} & i\sqrt{2}Q & i\sqrt{\frac{3}{2}}L & i\sqrt{2}M & D & 0 \\ i\sqrt{2}M^+ & -i\sqrt{\frac{3}{2}}L^+ & i\sqrt{2}Q & iL/\sqrt{2} & 0 & D \end{pmatrix}, \quad (\text{A1})$$

where $+$ ($-$) denotes a positive (negative) value of the complex part of k_3 , the component of \mathbf{k} along the Z quantization direction of the QW.

Let T be the resulting transfer matrix of the heterostructure. The requirement of the wave function to vanish at $Z = \pm \infty$ implies that the determinant of the 6×6 submatrix T_{ij} ($i, j = 1, \dots, 6$) must be zero. The determinantal equation gives implicitly the dispersion relation $E(k_{\parallel})$ for a given value of $k_{\parallel} = (k_1, k_2)$.

-
- ¹T. Hayakawa, M. Kondo, T. Suyama, K. Takahashi, S. Tamamoto, and T. Hijikata, *Jpn. J. Appl. Phys.* **26**, L302 (1987).
- ²A. G. Davies, J. E. Frost, D. A. Ritchie, D. C. Peacock, R. Newbury, E. H. Lindfield, M. Pepper, and G. A. C. Jones, *J. Cryst. Growth* **111**, 318 (1991).
- ³M. B. Santos, Y. W. Suen, M. Shayegan, Y. P. Li, L. W. Engel, and D. C. Tsui, *Phys. Rev. Lett.* **68**, 1188 (1992).
- ⁴R. K. Hayden, D. K. Maude, L. Eaves, E. C. Valadares, M. Henini, F. W. Sheard, O. H. Hughes, J. C. Portal, and L. Cury, *Phys. Rev. Lett.* **66**, 1749 (1991).
- ⁵O. H. Hughes, M. Henini, E. S. Alves, M. L. Leadbeater, L. Eaves, M. Davies, and M. Heath, *J. Vac. Sci. Technol. B* **7**, 1041 (1989).
- ⁶U. Gennser, V. P. Kesan, D. A. Syphers, T. P. Smith III, S. S. Iyer, and E. S. Yang, *Phys. Rev. Lett.* **67**, 3828 (1991).
- ⁷M. Henini, R. K. Hayden, E. C. Valadares, L. Eaves, G. Hill, and M. A. Pate, *Semicond. Sci. Technol.* **7**, 267 (1992); R. K. Hayden, E. C. Valadares, M. Henini, L. Eaves, D. K. Maude, and J. C. Portal (unpublished). The latter presents the hole subband surfaces $E(k_{\parallel})$ of a (311)A QW probed by RMTS which qualitatively agree with our calculation for $L_w = 60 \text{ \AA}$ using the γ 's of Ref. 12.
- ⁸R. K. Hayden, T. Takamasu, D. K. Maude, E. C. Valadares, L. Eaves, U. Ekenberg, N. Miura, M. Henini, J. C. Portal, G. Hill, and M. A. Pate, *Semicond. Sci. Technol.* **7**, B413 (1992).
- ⁹L. C. Andreani, A. Pasquarello, and F. Bassani, *Phys. Rev. B* **36**, 5887 (1987).
- ¹⁰J. M. Luttinger and W. Kohn, *Phys. Rev.* **97**, 869 (1955).
- ¹¹G. Bastard, J. A. Brum, and R. Ferreira, in *Solid State Physics: Semiconductor Heterostructures and Nanostructures*, edited by H. Ehrenreich and D. Turnbull (Academic, London, 1991), Vol. 44, p. 229.
- ¹²*Numerical Data and Functional Relationships in Science and Technology*, edited by O. Madelung, Landolt-Börnstein, New Series, Group III, Vol. 17 (Springer, Berlin, 1982).
- ¹³N. Binggeli and A. Baldereschi, *Phys. Rev. B* **43**, 14 734 (1991) and references therein.
- ¹⁴This is consistent with the absence of a measurable anisotropy in the conductivity of 2DHG on (311) interfaces. B. Gallagher (private communication).
- ¹⁵The density of states of a 2D saddle point ($E = E_{\text{SP}}$) diverges logarithmically with $|E - E_{\text{SP}}|$ whereas in 3D it varies linearly with E for $E > E_{\text{SP}}$ and as $|E - E_{\text{SP}}|^{1/2}$ for $E < E_{\text{SP}}$. N. W. Ashcroft and N. D. Mermin, *Solid State Physics* (CBS Publishing Asia Ltd., Philadelphia, 1976), p. 150.
- ¹⁶E. C. Valadares, F. W. Sheard, and L. Eaves, *Surf. Sci.* **267**, 409 (1992).
- ¹⁷R. Wessel and M. Altarelli, *Phys. Rev. B* **39**, 12 802 (1989).

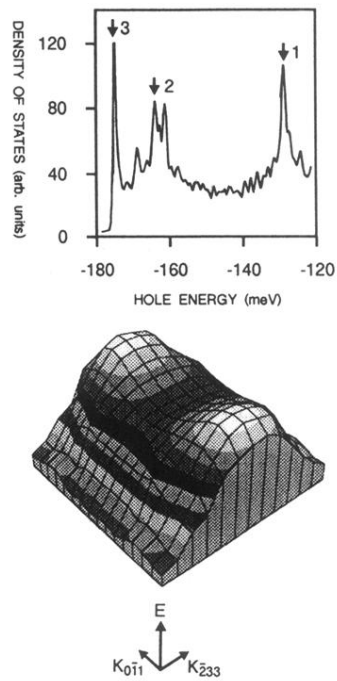


FIG. 3. Saddle point displayed by the fourth (iv) subband of Fig. 2(b) and the corresponding density of states (DOS). Arrow number 1 indicates the saddle-point energy (see text). The lack of smoothness of this curve is due to the method used to calculate the DOS, based on a histogram counting of states.